Harnessing random low Reynolds number flow for net migration

Takeru Morita,[1] Toshihiro Omori,[1] Yohei Nakayama,[2] Shoichi Toyabe,[2] and Takuji Ishikawa [1,3,*]

[1]*Department of Fine Mechanics, Graduate School of Engineering, Tohoku University 6-6-01 Aoba, Aramaki, Aoba-ku, Sendai 980–8579, Japan*

[2]*Department of Applied Physics, Graduate School of Engineering, Tohoku University 6-6-05 Aoba, Aramaki, Aoba-ku, Sendai 980–8579, Japan*

[3]*Graduate School of Biomedical Engineering, Tohoku University 6-6-01 Aoba, Aramaki, Aoba-ku, Sendai 980–8579, Japan*

Random noise in low Reynolds number flow has rarely been used to obtain net migration of microscale objects. In this study, we numerically show that net migration of a microscale object can be extracted from random directional fluid forces in Stokes flow, by introducing deformability and inhomogeneous density into the object. We also developed a mathematical framework to describe the deformation-induced migration caused by noise. These results provide a basis for understanding the noise-induced migration of a microswimmer and are useful for harnessing energy from low Reynolds number flow.

I. INTRODUCTION

Fluid motion often contains some randomness. In turbulent flow, for example, the kinetic energy cascades from the large scale to smaller scales. Technologies to channel the power of random flow energies, such as wind, wave, and tidal current, basically utilize high Reynolds number flow. In low Reynolds number flow, on the other hand, conventional technologies may not be applicable, because the kinetic energy is no longer transported by convection, but dissipates instantaneously. Thus, the ability to harness energy from low Reynolds number random flow is still largely unexplored. Moreover, random noise in low Reynolds number flow has rarely been used to obtain net migration of microscale objects, such as natural microorganisms and artificial microswimmers. The random noise considered here can be generated, for example, by turbulent flow and by randomly shaking a tank containing the object.

Simple reciprocal body deformation cannot induce net migration in Stokes flow, as stated in the Scallop theorem [1,2]. Hence, natural swimming microorganisms produce non-reciprocal motions using their swimming apparatus, such as flagella and cilia. Their swimming mechanisms have been investigated widely over the past half century [3–6]. Although swimming microorganisms can accumulate in a certain spot by interacting with the background flow field [7–9], cells rarely utilize the random noise of flow for their migration.

Recently, artificial microswimmers have attracted the attention of many researchers due to their potential importance in engineering and medical applications [10]. Most microswimmers utilize magnetic forces [11,12], electric forces [13], chemical forces [14], optical forces [15], or phoretic forces [16,17] for propulsion. Although a microswimmer is strongly affected by the surrounding flow field, only a few

studies have utilized fluid forces for propulsion. Vladimirov [18] and Ishikawa and Vladimirov [19] showed that the net migration of a dumbbell microrobot can be induced by controlling fluid oscillations. However, those studies did not utilize the random noise of the flow for net migration, such as the shear and body forces induced on a microswimmer by the surrounding flow that fluctuates over space and time, though fluid motion in nature often contains random noise.

In this paper, we numerically demonstrate that the net migration of a microscale object can be determined based on random directional fluid body forces and the deformability of the object. Our results show that under gravity, the object could migrate vertically downward when random forces were applied, although the object as a whole was neutrally buoyant and there was no sedimentation effect. The migration mechanism can be understood according to nonreciprocal body deformation in Stokes flow. We also developed a mathematical model to describe the net migration induced by random fluid forces; this model is capable of predicting behaviors of deformable objects under various conditions, and illustrated that drag asymmetry acts like a ratchet to generate net motion under noise. The results described below provide a basis for understanding noise-induced migration and are useful for harnessing energy from low Reynolds number flow.

II. METHODS

A. Microcapsule

The microscale object used in the simulation is similar to that described in our previous papers [20,21]. The microcapsule consists of an elastic membrane with a prolate spheroidal reference shape. It contains a rigid sphere that is connected to the capsule membrane by linear springs, as shown in Fig. 1(a). The lengths of the major and minor axes of the reference shape are a_1 and a_2, respectively. We assume that the densities of the surrounding fluid ρ_∞, the fluid inside the capsule ρ_c, and the
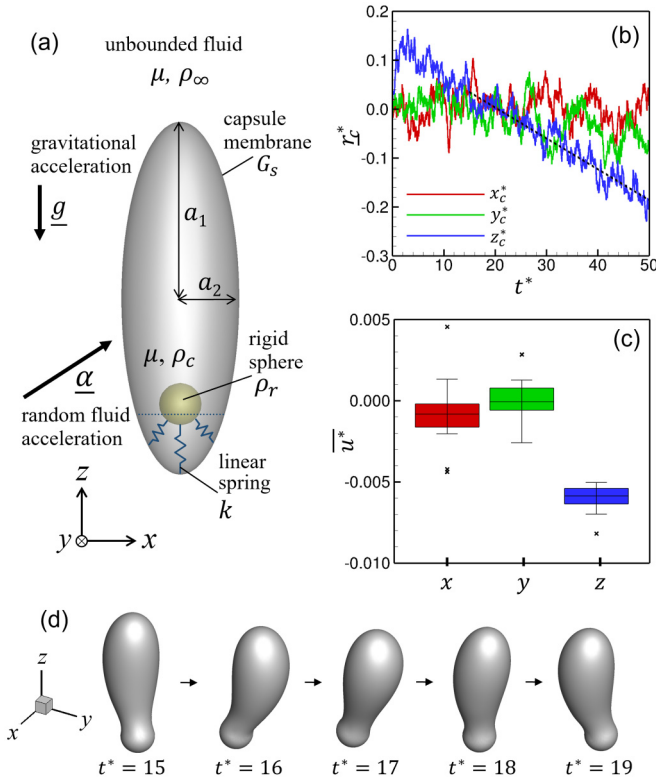
_____
*Corresponding author: ishikawa@bfsl.mech.tohoku.ac.jp

FIG. 1. Vertical propulsion of the microcapsule by random fluid forces ($a_1/a_2 = 3, A = 10$, $\tau^* = 3.15 \times 10^{-3}$ and Bo = 1) (a) Schematic diagram of the microcapsule and problem settings. The gravitational acceleration g is imposed in the $-z$ direction. The dotted line on the capsule indicates the area under which the spring forces were considered. (b) Time change of the x, y, and z components of the volume center. The broken line indicates the slope of z_c^*, which is calculated by the method of least squares in the range $15 \leqslant t^* \leqslant 50$. (c) Box plots of the propulsion velocities in the $x, y,$ and z directions. Sixteen independent simulation cases were examined; the symbol ' $\times$ ' indicates the outliers. (d) Sample snapshots of the deformed microcapsule from $15 \leqslant t^* \leqslant 19$ (please see Supplemental Material Movie 1).

rigid sphere ρ_r satisfy the inequality $\rho_c < \rho_\infty < \rho_r$, although the average density of the whole capsule is equivalent to the surrounding fluid. For simplicity, the viscosities, μ, of the surrounding fluid and the fluid inside the capsule are assumed to be identical.

Gravity acts in the negative z direction. If there is no gravity, the microcapsule does not have any preferred direction and migrates to any direction with equal probability. Thus, the ensemble averaged migration velocity becomes zero. In order to extract nonzero ensemble averaged migration, gravity is introduced in this study. Besides, gravity is unavoidable on earth.

B. Random fluid forces

The background flow is assumed to randomly change its direction, which produces a random acceleration field. Such an acceleration field can also be created by shaking a tank containing the microcapsule. We further assumed that the size of the microcapsule is sufficiently smaller than the length scale

of the background flow. Hence, we can model the background noise as the random acceleration field acting on the entire system. We note that, in the absence of the microcapsule, bulk fluid shows a rigid body motion and no rate of strain is generated by the acceleration field. The acceleration field produces body forces that are in opposition to the fluid inside the capsule and the rigid sphere, due to the density mismatch. These opposing fluid forces deform the capsule, which results in nonreciprocal body deformation and net migration. Deformation-based migration has been examined in several former studies [22–27]; however, none of these investigations harnessed random fluid forces for net migration.

To introduce random noise with time correlation, we generated autocorrelated pseudorandom numbers, K_t, using the following equation [28]:

$$K_t = \frac{(1-\lambda)B_t + \lambda K_{t-\Delta t}}{\sqrt{(1-\lambda)^2 + \lambda^2}}, \qquad (1)$$

where t is time. B_t is a Gaussian random number generated by a Box-Muller transform [29], which has zero mean with variance of 1. λ is a parameter controlling the relaxation time, satisfying $0 \leqslant \lambda \leqslant 1$. K_t also has a zero mean with a variance of 1. The initial value of K_t was set as $K_0 = B_0$. The time correlation of K_t decays exponentially, and the relaxation time τ can be mathematically derived as

$$\tau = -\frac{\Delta t}{\ln \phi(\lambda)} \quad , \quad \phi(\lambda) = \frac{\lambda}{\sqrt{(1-\lambda)^2 + \lambda^2}}, \qquad (2)$$

where Δt is the time step of computation. The random acceleration field $\underline{\alpha}$ is then given by

$$\underline{\alpha} = (|\underline{g}|A_x K_{t,1}, \; |\underline{g}|A_y K_{t,2}, \; |\underline{g}|A_z K_{t,3}), \qquad (3)$$

where g is the gravitational acceleration, A_i is the amplitude in the i direction, and $K_{t,1}$, $K_{t,2}$, and $K_{t,3}$ are an independent series of pseudorandom numbers.

C. Governing equations

The governing equations are similar to those used in our previous studies [20,21]. Due to the small size of the microcapsule, we neglected inertial effects on the fluid flow, as well as the capsule motion. Solutions were determined for the following: (1) the flow field inside and outside the capsule using the governing equations for Stokes flow, (2) membrane deformation using the governing equations for solid mechanics, and (3) the motion of the rigid sphere based on the force and torque conditions. The membrane was modeled as a two-dimensional hyperelastic material, in which the Skalak model [30] was employed as a constitutive law of the in-plane stretch and the Helfrich model [31] was applied for bending rigidity.

The governing equations are nondimensionalized using characteristic length a_c, defined as $a_c = \sqrt[3]{a_1 a_2^2}$, characteristic velocity $|\rho_c - \rho_\infty|g a_c^2/\mu$, and the membrane's shear elastic modulus G_s that appears in the Skalak law [30]. In this paper, symbol * indicates a nondimensionalized quantity.

D. Numerical methods and parameters

We used a numerical approach similar to that described in our previous studies [20,21]. Briefly, the solid mechanics of the membrane were solved using a finite element method, and the fluid mechanics of the inner and surrounding fluids were solved by a boundary element method. For time marching, we used a second-order Runge-Kutta method, with a time step of $\Delta t = 5.0 \times 10^{-5}$. The capsule membrane was divided into 5,120 triangular elements, and the rigid sphere surface was divided into 320 triangular elements. The density ratio between the rigid sphere and the fluid inside the capsule was set as $\rho_r / \rho_c = 20$. The volume ratio of the whole microcapsule to the rigid sphere was set as 4^3. We set the bending rigidity and the spring parameters as $E_b / G_s a_c^2 = 0.1$ and $k_s a_c^2 / G_s = 100$, where E_b is the bending modulus of the Helfrich model [31] and k_s is the spring strength. The feasibility of these parameters was discussed in detail in our previous paper [20].

In this study, we investigated the effect of four major parameters on the net migration: the amplitude of random fluid oscillation A ($= A_x = A_y = A_z$); the relaxation time τ; the aspect ratio of the reference shape a_1 / a_2; and the Bond number $\text{Bo} = |\rho_c - \rho_\infty| a_c^2 g / G_s$, a dimensionless number indicating the ratio of the gravitational force to the elastic force.

III. RESULTS

Figure 1(b) shows the change in volume center of the capsule $r_{\underline{c}}^*$ over time, where the relaxation time is set as $\tau^* = 3.15 \times 10^{-3}$. The vertical component z_c^* decreases gradually over time, indicating vertically downward migration of the capsule. Figure 1(c) shows box plots of 16 independent simulations with different random forces. Although no clear migration was observed horizontally, i.e., in the x and y directions, clear downward migration was observed in all cases. During migration, the capsule becomes deformed, as shown in Fig. 1(d) (see also Supplemental Material Movie 1 [32]); the mechanism responsible for downward migration has yet to be determined.

To clarify the migration mechanism, we performed a trial simulation without a vertical component to the random force. The capsule migration results are shown in Fig. 2(a); we can see that the migration velocity induced only by horizontal forces ($A_z = 0$, $A_x = A_y = 10$) is similar to that induced by the full three-dimensional (3D) forces. Moreover, even unidirectional horizontal forces ($A_y = A_z = 0$, $A_x = 10$) can generate moderate downward migration. The migration velocity when $A_y = A_z = 0$ is about half that when $A_z = 0$, indicating that the effects of the horizontal forces are nearly superimposed. These results illustrate that the downward migration is generated mainly by random horizontal forces.

To investigate the mechanism further, we performed another trial simulation by setting sinusoidal oscillation forces only in the x direction, i.e., $\underline{\alpha} = (|g| A'_x \cos(2\pi t / T), 0, 0)$, as shown in Fig. 2(b). The red curve in Fig. 2(c) shows the resultant change in the z position during the half period of oscillation, in which the rigid sphere moves from the center to the right and then back to the center. A large reduction in the z position can be seen in the first quarter, i.e., where the rigid sphere moves from the center to the right end, whereas
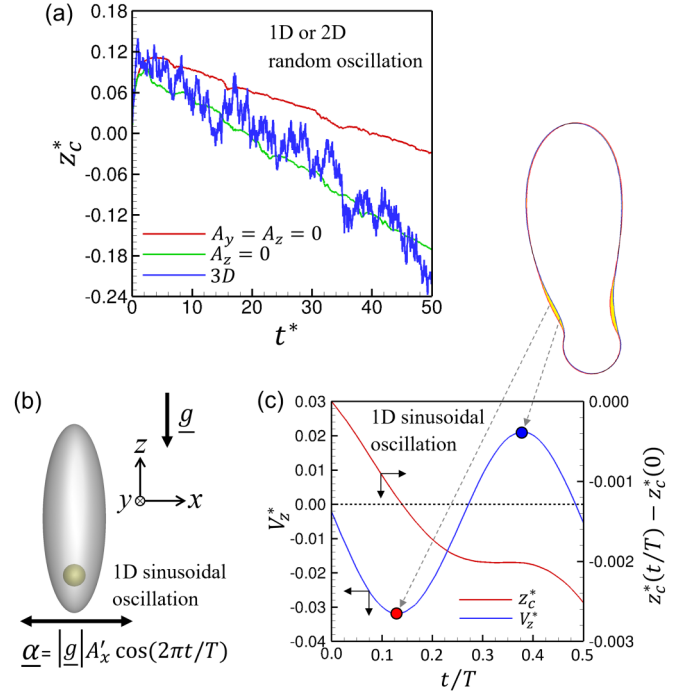

FIG. 2. Migration mechanism (a) Time change of the z component of the volume center under different random force conditions ($a_1 / a_2 = 3$, $\tau^* = 3.15 \times 10^{-3}$ and $\text{Bo} = 1$). In the figure, $A_y = A_z = 0$ indicates the case with only x-directional random forces ($A_y = A_z = 0$, $A_x = 10$), $A_z = 0$ indicates the case with horizontal random forces in the $x - y$ plane ($A_z = 0$, $A_x = A_y = 10$), and 3D indicates the case with full three-dimensional random forces ($A = 10$). (b),(c) Vertical propulsion of the microcapsule under uniaxial sinusoidal oscillations in the x direction ($a_1 / a_2 = 3$, $A'_x = 10$, $T^* = 1$ and $\text{Bo} = 1$). (b) Schematic diagram of the problem settings. The acceleration $\underline{\alpha}$ of the oscillating fluid is horizontal, sinusoidal, and unidirectional in the x direction. (c) The propulsion mechanism of the microcapsule. The red curve indicates the actual change of z_c^* during a half period of oscillation in the simulation. The blue curve indicates the vertical propulsion velocity V_z^*, which was obtained by assuming rigid body motion under a given shape and torque. Inset figures show the shape of the capsule at the peak velocity. Red and blue curves indicate the shapes at red and blue points; the difference in shape is shown in yellow.

in the second quarter a smaller change in the z position is observed, as the rigid sphere moves from the right end to the center. Thus, the capsule motion is no longer reciprocal. Such a nonreciprocal body motion results in net migration even in the Stokes flow regime.

Around the middle point between the center and the right end, the capsule shows deformation [Fig. 2(c)]. Although the difference in shapes is small, a difference in migration velocity occurs. To isolate the shape effect (i.e., exclude the surface velocity effect), we conducted a trial run to calculate the vertical propulsion velocity V_z by assuming that the capsule shows rigid body motion under a given torque induced by the oscillation forces. The results are also plotted as the blue curve in Fig. 2(c). A large downward velocity can be seen in the first quarter, and a small upward velocity in the second quarter, which illustrates that asymmetry in migration
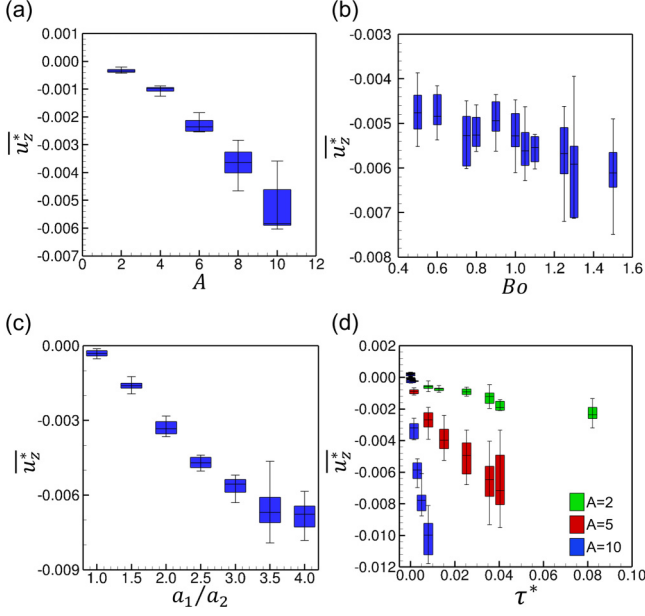
FIG. 3. Effects of parameters on the average vertical migration velocity $\overline{u_z^*}$. Each plot consists of 12 independent simulation cases. Effect of (a) amplitude A (Bo $= 1$, $a_1/a_2 = 3$ and $\tau^* = 3.15 \times 10^{-3}$), (b) Bond number Bo, which indicates the deformability of the capsule ($A = 10$, $a_1/a_2 = 3$ and $\tau^* = 3.15 \times 10^{-3}$), (c) the aspect ratio a_1/a_2 ($A = 10$, Bo $= 1$ and $\tau^* = 3.15 \times 10^{-3}$), and (d) the relaxation time τ^* (Bo $= 1$, $a_1/a_2 = 3$), where blue indicates $A = 10$, red indicates $A = 5$, and green indicates $A = 2$.

can arise even with small changes in the deformed shape. The upward velocity of the rigid body motion was not observed in the full simulation; this indicates that the surface velocity due to deformation plays an important role in migration.

The effects of various parameters on the average vertical migration velocity $\overline{u_z^*}$ were investigated and are shown in Fig. 3, where A is the amplitude of the random force,

Bond number Bo is a dimensionless number indicating the deformability of the capsule, a_1/a_2 is the aspect ratio, and τ is the relaxation time of the random force. We note that when Bo is zero $\overline{u_z^*}$ is also zero, because there is no gravity effect. Downward migration is clearly enhanced by an increase in all of the parameters in the investigated regimes. The effects of A, a_1/a_2, and τ are especially significant. Because the capsule shows larger deformation with increasing A, a_1/a_2, and τ, deformation plays a key role in the migration. We can conclude that large, nonreciprocal deformation is required for effective extraction of the net migration of a deformable object from random directional fluid forces.

IV. THEORY

Here we propose a simple theory to explain qualitatively the numerical results obtained, and to provide a general picture of the deformation-induced migration caused by noise. We also compare the consequences of the mathematical model to the present numerical results.

The deformation-induced migration caused by noise can be modeled as follows:

$$\Gamma(\Pi)\frac{dz_c}{dt} = C_z\xi, \tag{4}$$

$$\gamma\frac{d\Pi}{dt} = -\frac{\partial U(\Pi)}{d\Pi} + C_\Pi\xi, \tag{5}$$

where Π is the coordinate expressing the deformation, Γ is a component of the viscous drag tensor of translational motion, γ is the viscous drag coefficient for deformation, U is the potential for deformation, C_z and C_Π are numerical coefficients, and ξ is the random force. We neglected inertia effects, given that the flow is Stokesian, and the equations are overdamped.

By assuming small deformation near the equilibrium shape, we can linearize the equations and derive the asymptotic solution as follows:

$$\left\langle\frac{dz_c}{dt}\right\rangle = \left\langle C_z\left(\frac{1}{\Gamma(\Pi^\#)} - \frac{\Gamma'(\Pi^\#)}{\Gamma(\Pi^\#)^2}\frac{1}{\gamma}\int_{-\infty}^{t}d\hat{t}\exp\left[-\frac{k}{\gamma}(t-\hat{t})\right]C_\Pi\xi(\hat{t})\right)\xi(t)\right\rangle$$

$$= -\frac{C_zC_\Pi}{\gamma\,\Gamma(\Pi^\#)^2}\frac{d\,\Gamma(\Pi^\#)}{d\,\Pi}\int_{-\infty}^{t}d\hat{t}\exp\left[-\frac{k}{\gamma}(t-\hat{t})\right]\langle\xi(\hat{t})\xi(t)\rangle, \tag{6}$$

where $\langle\;\rangle$ indicates the ensemble average, $\Pi^\#$ is the equilibrium shape of the capsule with the minimum potential energy, and $k = d^2U(\Pi^\#)/d\Pi^2$. This equation indicates that $d\Gamma(\Pi^\#)/d\Pi$ must be nonzero to generate the required migration velocity. In other words, asymmetric viscous drag around the equilibrium shape is necessary for net migration, which cannot be achieved by a rigid object. In the case of the present microcapsule, asymmetric viscous drag is generated between stretching and compressing capsules, which may act like a ratchet to generate the net downward motion under noise.

Equation (6) also indicates that the migration velocity is related to the random force correlation $\langle\xi(\hat{t})\xi(t)\rangle$. The random force considered here is similar to that used in the simulation,

and is assumed to be Gaussian noise with relaxation time τ, satisfying the following equation:

$$\langle\xi(\hat{t})\xi(t)\rangle = A^2\exp\left(-\frac{|\hat{t}-t|}{\tau}\right). \tag{7}$$

Equation (6) can then be transformed as follows:

$$\left\langle\frac{dz_c}{dt}\right\rangle \propto \frac{1}{k}\frac{A^2}{\left(1+\frac{\tau_d}{\tau}\right)}. \tag{8}$$

Here, $\tau_d = \gamma/k$ is the relaxation time of the deformation. This equation indicates that the migration velocity is determined by the ratio of the relaxation time of the random forces τ to that of the deformation τ_d. The migration is enhanced
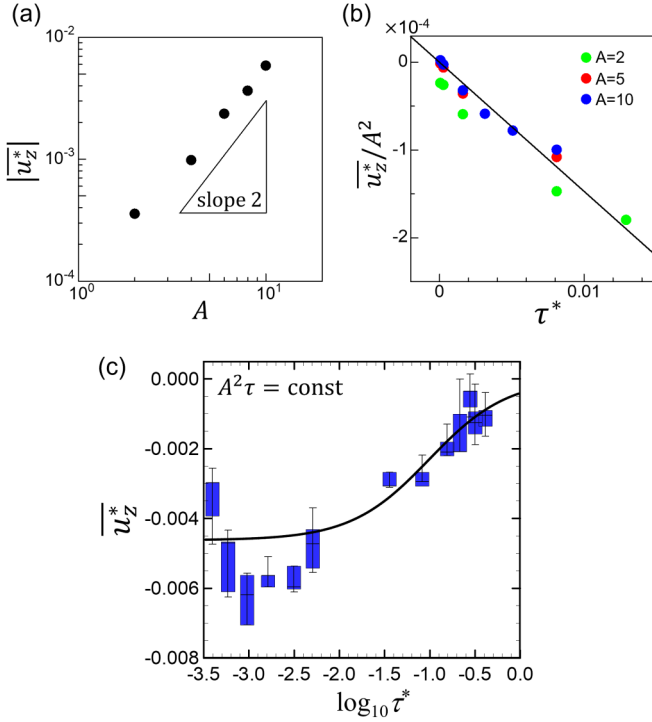
FIG. 4. The average vertical migration velocity $\overline{u_z^*}$ based on the proposed theory. (a) Effect of amplitude A on the magnitude of $\overline{u_z^*}$, plotted in log-log scale (Bo = 1, $a_1/a_2 = 3$ and $\tau^* = 3.15 \times 10^{-3}$). Each plot is a median value of 12 independent simulation cases. Slope 2 is drawn for comparison. (b) Effect of the relaxation time τ^* on $\overline{u_z^*}/A^2$ (Bo = 1, $a_1/a_2 = 3$). A line passing through the origin is plotted using the least squares method (slope $c_0 = -1.47 \times 10^{-2}$, $r = 0.967$). (c) Effect of relaxation time τ^* on $\overline{u_z^*}$ under the condition of $A^2\tau = 0.315$ (Bo = 1, $a_1/a_2 = 3$). Function $c_0 A^2 \tau /(1 + \tau/\tau_d)$ is plotted by the least squares method ($\tau_d = 0.098$, $r = 0.882$).

as the deformation relaxation becomes faster than the random force relaxation. A quick deformation response relative to the force change may act like a ratchet to generate net migration under noise.

Now we compare Eq. (8) with the numerical results. Equation (8) indicates that the migration velocity increases with the random force strength A and relaxation time τ. These basic tendencies were observed in Fig. 3. The quadratic dependency of the migration velocity with A is confirmed, as shown in Fig. 4(a). Because k is the second derivative of U with respect to Π at the equilibrium shape, a small k represents large deformability. We observed in Fig. 3 that migration velocity increases with the degree of deformability, i.e., k is reduced, which is again consistent with Eq. (8).

Regarding the small τ limit, Eq. (8) can be transformed to $\langle \dot{z}_c \rangle \propto \tau$; the data shown in Fig. 3(d) may collapse into a single line in the $\frac{\overline{u_z^*}}{A^2} - \tau^*$ plot. The results are shown in Fig. 4(b). The figure shows that the migration velocity is nearly proportional to the relaxation time. The data when $A = 2$, 5, or 10 almost collapse into a single line, which indicates that the values of k and γ are similar, regardless of A. We note that the data points shown in the figure satisfy $\tau^* \ll \tau_d$, where τ_d is estimated as 0.098 in the next paragraph. These results

illustrate that migration does not occur when $\tau \to 0$ with a finite value of A.

The power of the random fluctuating force corresponds to $A^2 \tau$. The migration velocity increases as τ decreases, while keeping $A^2\tau$ constant, as shown in Fig. 4(c). By rewriting Eq. (8), we have

$$\left\langle \frac{dz_c}{dt} \right\rangle \propto \frac{1}{\gamma} \frac{A^2\tau}{\left(1 + \frac{\tau}{\tau_d}\right)}. \tag{8a}$$

That is, the theory predicts that the migration velocity is determined by the power $A^2\tau$, the ratio of relaxation time τ/τ_d, and the frictional coefficient γ. We fitted a curve $c_0 A^2 \tau /(1 + \tau/\tau_d)$ using the least squares method, as shown in Fig. 4(c), where $A^2\tau = 0.315$. The coefficient c_0 is obtained from the fitted line in Fig. 4(b) as $c_0 = -1.47 \times 10^{-2}$. Hence, the fitted parameter here is only τ_d, and the value was estimated as 0.098. The estimated value of τ_d is of the same order of magnitude as the deformation relaxation time under a periodic oscillation condition of $\tau_d = 0.14$ (cf. Morita *et al.* [20]). Thus, our simple model provides a good representation of the system.

V. DISCUSSIONS

Noise-induced transport and ratchets, such as pulsating ratchets, tilting ratchets, molecular motors, and quantum ratchets, have been intensively investigated in theoretical and experimental physics [33–35]. Most of previous studies rectified thermal fluctuation for the unidirectional migration by utilizing asymmetric potential. On the other hand, we achieved the rectification by exploiting asymmetric friction. Notably, the deformation of the object generates the frictional asymmetry, which is a unique rectification mechanism.

Last, we estimate quantitatively the migration speed. In dimensionless form, the maximum migration velocity we observed was about 0.01 [cf. Fig. 3(d)]. The velocity is nondimensionalized by the characteristic velocity of $|\rho_c - \rho_\infty| g a_c^2/\mu$. By assuming that the surrounding fluid to be 0.9 wt. % normal saline, the density and the viscosity can be estimated approximately as $\rho_\infty = 1.0 \times 10^3$ kg/m^3 and $\mu = 1.0$ mPa s at 20 °C. For this example, the fluid inside the capsule is taken to be oil and the rigid sphere is taken to be an alloy. The density of silicon oil can be $\rho_c = 7.6 \times 10^2$ kg/m^3 at 20 °C, and the density of a specific titanium-gold alloy can be $\rho_r = 1.6 \times 10^4$ kg/m^3. Furthermore, by assuming the radius of the microcapsule to be $a_c = 100 \, \mu$m, we can derive $|\rho_c - \rho_\infty| g a_c^2/\mu = 23.5$ mm/s. Thus, the dimensionless velocity of 0.01 corresponds to 235 μm/s. These results illustrate that the present mechanism has potential to generate large migration velocity.

VI. CONCLUSIONS

In this paper, we showed that net migration of a deformable object in Stokes flow can be extracted from random fluid forces. We also provided a mathematical framework to describe the deformation-induced migration caused by noise. The proposed theory was able to predict the effect of various parameters on the net migration, and the importance of asymmetric viscous drag around the equilibrium shape, i.e.,

a ratchet, for net migration. The results provide a basis for understanding the noise-induced migration of a microswimmer and are useful for harnessing energy from low Reynolds number flow.

[1] E. M. Purcell, Life at low Reynolds number, Am. J. Phys. **45**, 3, (1977).

[2] E. Lauga, Life around the scallop theorem, Soft Matter **7**, 3060, (2011).

[3] C. Brennen and H. Winet, Fluid mechanics of propulsion by cilia and flagella, Annu. Rev. Fluid Mech. **9**, 339 (1977).

[4] T. Ishikawa, Suspension biomechanics of swimming microbes, J. R. Soc. Interface **6**, 815 (2009).

[5] E. Lauga and T. R. Powers, The hydrodynamics of swimming microorganisms, Rep. Prog. Phys. **72**, 096601 (2009).

[6] R. E. Goldstein, Green algae as model organisms for biological fluid dynamics, Annu. Rev. Fluid Mech. **47**, 343 (2015).

[7] J. S. Guasto, R. Rusconi, and R. Stocker, Fluid mechanics of planktonic microorganisms, Annu. Rev. Fluid Mech. **44**, 373 (2012).

[8] W. M. Durham, J. O. Kessler, and R. Stocker, Disruption of vertical motility by shear triggers formation of thin phytoplankton layers, Science **323**, 1067 (2009).

[9] F. De Lillo, M. Cencini, W. M. Durham, M. Barry, R. Stocker, E. Climent, and G. Boffetta, Turbulent Fluid Acceleration Generates Clusters of Gyrotactic Microorganisms, Phys. Rev. Lett. **112**, 044502 (2014).

[10] K. E. Peyer, L. Zhang, and B. J. Nelson, Bio-inspired magnetic swimming microrobots for biomedical applications. Nanoscale **5**, 1259 (2013).

[11] R. Dreyfus, J. Baudry, M. L. Roper, M. Fermigier, H. A. Stone, and J. Bibette, Microscopic artificial swimmers, Nature (London) **437**, 862 (2005).

[12] J. Li, B. E. F. de Ávila, W. Gao, L. Zhang, and J. Wang, Micro/nanorobots for biomedicine: Delivery, surgery, sensing, and detoxification, Sci. Robot. **2**, eaam6431 (2017).

[13] G. Loget and A. Kuhn, Electric field-induced chemical locomotion of conducting objects, Nat. Commun. **2**, 535 (2011).

[14] H.-R. Jiang, N. Yoshinaga, and M. Sano, Active Motion of a Janus Particle by Self-Thermophoresis in a Defocused Laser Beam, Phys. Rev. Lett. **105**, 268302 (2010).

[15] J. Li *et al.*, Swimming microrobot optical nanoscopy, Nano Lett. **16**, 6604 (2016).

[16] R. Golestanian, T. B. Liverpool, and A. Ajdari, Designing phoretic micro- and nano-swimmers. New J. Phys. **9**, 126 (2007).

[17] J. Elgeti, R. G. Winkler, and G. Gompper, Physics of microswimmers - single particle motion and collective behavior: A review, Rep. Prog. Phys. **78**, 056601 (2015).

[18] V. A. Vladimirov, Dumbbell micro-robot driven by flow oscillations, J. Fluid Mech. **717**, R8 (2013).

[19] T. Ishikawa and V. A. Vladimirov, A stepping microrobot controlled by flow oscillations, J. Fluids Eng. **137**, 084501 (2015).

[20] T. Morita, T. Omori, and T. Ishikawa, Passive swimming of a microcapsule in vertical fluid oscillation, Phys. Rev. E **98**, 023108 (2018).

[21] T. Morita, T. Omori, and T. Ishikawa, Biaxial fluid oscillations can propel a micro-capsule swimmer in an arbitrary direction, Phys. Rev. E **98**, 063102 (2018).

[22] A. Shapere and F. Wilczek, Self-Propulsion at Low Reynolds Number, Phys. Rev. Lett. **58**, 2051 (1987).

[23] J. E. Avron, O. Gat, and O. Kenneth, Optimal Swimming at Low Reynolds Numbers, Phys. Rev. Lett. **93**, 186001 (2004).

[24] A. Farutin, S. Rafaï, D. K. Dysthe, A. Duperray, P. Peyla, and C. Misbah, Amoeboid Swimming: A Generic Self-Propulsion of Cells in Fluids by Means of Membrane Deformations, Phys. Rev. Lett. **111**, 228102 (2013).

[25] H. Wu, M. Thiebaud, W. F. Hu, A. Peyla, and C. Misbah, Amoeboid motion in confined geometry, Phys. Rev. E **92**, 050701(R) (2015).

[26] H. Wu *et al.*, Amoeboid swimming in a channel, Soft Matter **12**, 7470 (2016).

[27] B. Nasouri, A. Khot, and G. J. Elfring, Elastic two-sphere swimmer in Stokes flow, Phys. Rev. Fluids **2**, 043101 (2017).

[28] V. C. Lakhan, Generating autocorrelated pseudorandom numbers with specific distributions, J. Statist. Comput. Simul. **12**, 303 (1981).

[29] G. E. P. Box and M. E. Muller, A note on the generation of random normal deviates, Ann. Math. Stat. **29**, 610 (1958).

[30] R. Skalak, A. Tozeren, R. P. Zarda, and S. Chien, Strain energy function of red blood cell membranes, Biophys. J. **13**, 245 (1973).

[31] W. Helfrich, Elastic properties of lipid bilayers: Theory and possible experiments, Z. Naturforsch. **28**, 693 (1973).

[32] See Supplemental Material at http://link.aps.org/supplemental/10.1103/PhysRevE.101.063101 for sample movie of vertical propulsion of the microcapsule by random fluid forces.

[33] P. Reimann, Brownian motors: Noisy transport far from equilibrium, Phys. Rep. **361**, 57 (2002).

[34] M. O. Magnasco, Forced Thermal Ratchets, Phys. Rev. Lett. **71**, 1477 (1993).

[35] J. Rousselet, L. Salome, A. Ajdari, and J. Prost, Directional motion of brownian particles induced by a periodic asymmetric potential, Nature (London) **370**, 446 (1994).